

## **Phosphoric acid activation of titanium-supported lead dioxide electrodes for bipolar battery applications**

A. Kirchev\*(0000-0001-5553-9319), L. Serra, B. Marie

Univ. Grenoble Alpes, CEA, Liten, Campus Ines, 50 Av. de Lac Leman, 73375 Le Bourget du Lac, France

\*corresponding author e-mail: angel.kirchev@cea.fr

### **Abstract**

Titanium foil coated with doped tin dioxide is attractive option for positive current collector interface of bipolar lead batteries due its corrosion resistance and mechanical performance. The phosphoric acid and two of its derivatives, one inorganic (calcium hydrogen phosphate) and one organic (poly-vinylphosphonic acid), have been studied as additives with potential for improvement of the capacity retention of such positive electrodes. The results show that the jar-formation process of the electrodes in the sulfuric acid electrolyte containing phosphoric acid overcomes successfully the capacity retention problem at all studied cases. It leads also to considerable improvement of the lead dioxide utilization. The cycling ageing of the electrodes combined with periodic impedance spectroscopy measurements, indicate progressive capacity loss corresponding to the typical processes of degradation of the lead dioxide structure. A rather small changes in the electrode resistance prove the corrosion and the passivation resistance of the current collectors. It is concluded that the combined doping with phosphoric acid species in the electrolyte and in the positive paste offers a potential for further improvements of the electrodes cyclability.

**Key words:** lead dioxide electrode, bipolar lead-acid battery, titanium current collectors, phosphoric acid, poly-vinylphosphonic acid

## Introduction

The electrification of the personal transport and the increasing deployment of renewable energy sources during the last decade resulted in tremendous growth of the energy storage market, from roughly 320 GWh produced in 2010 to more than 1500 GWh estimated for 2025 [1]. Considering the ambitions of the most of the developed countries to reach nearly total decarbonization of their economics in 2050, it is expected that the needs for the energy storage will grow even faster. Meeting such demand is nearly impossible task for a single type of energy storage technology taking into account the limited abundance of elements like lithium, copper, nickel, cobalt and vanadium, which are amongst the basic components of the Lithium-ion, Sodium-ion and Redox-Flow batteries [2]. Unlike these elements which are already used in a wide spectrum of applications different from the energy storage, the lead-acid batteries are relying principally on only one metal – the lead. The toxicity of this element reduced its uses to a small number of applications, the energy storage being the one which consumes about 90% of its global production [3]. The toxicity of the lead resulted also in very strict environmental regulations over all industries using this element. One of the most important outcomes from such a measure was the increase of the lead-acid battery recycling process efficiency above 99% considering the total battery weight and over 99.9% considering the lead metal itself [4]. The lead-acid battery electrochemistry offers several more key-point advantages over the above-mentioned competing electrochemical systems – it is intrinsically safe, it possesses a wide temperature tolerance, its self-discharge is rather low and it may operate with energy efficiency reaching 85 - 90% [5, 6]. These strong points make the lead-acid technologies very attractive for stationary applications due to their rather low demand for energy density. However, the lead-acid batteries still suffer one major drawback – a limited cycle and calendar life time, the latter depending strongly on the particular design of the positive electrodes and the type of the separator system used [7]. The positive electrodes degradation is driven by two processes taking place in parallel – the anodic corrosion of the lead alloy current collector and the loss of integrity of the porous lead dioxide due to the charge/discharge cycling denoted as “softening” and “shedding” of the positive active material (PAM).

The replacement of the lead alloy positive current collectors with titanium as a corrosion mitigation measure has been first proposed by Faber [8] shortly after the success of the dimensionally stabilized anodes (DSA) technology [9] and the start of some large-scale, cost-efficient production of metallic titanium. The essence of the DSA technology is based on the ability of the titanium to form solid oxide solutions with other metals when the difference in the ionic radius of Ti(IV) and the other metallic cation is less than 15%. In this way, the titanium surface can be coated with semi-conductive oxide layer with strong adhesion coming from the formation of the mixed oxide interface ( $\text{TiO}_2\text{-MeO}_x$ ) between the metallic titanium and the corresponding oxide [9]. When the outer metal oxide coating is conductive, but not electro-catalytic, for example  $\text{SnO}_2$  doped with F or Sb [10], it can be further electroplated with dense layer of  $\text{PbO}_2$  which may act as an artificial corrosion layer of the titanium positive grid.

The chemically pure titanium can be rolled to foil with low thickness (e.g.  $< 100\mu\text{m}$ ) with mechanic performance similar to its copper or aluminum counterparts in terms of tensile and puncture strength [11]. This combination of high strength and corrosion resistance has been found very useful in the development of bipolar lead-acid batteries [12, 13]. Since the titanium is susceptible to cathodic corrosion at electrode potentials more negative than 0V vs. standard hydrogen electrode (SHE) [11], the corresponding bipolar current collectors should be composed of  $\text{SnO}_2$  coated titanium foil laminated together with lead or lead alloy foil interfacing the negative active material (NAM). The research carried out on such type of bipolar current collectors demonstrated the equivalent of 28

years of operation in floating charge at 2.3 V/cell and 25°C for SnO<sub>2</sub> coatings thicker than 100 nm [14]. This result indicates that the use of titanium current collector practically resolves the lead-acid battery failure modes driven by the corrosion process.

The possibility to use very thin (< 100 μm) expanded titanium mesh as current collector for thin-plate lead-acid batteries has been also studied recently [15]. The decreased electrode thickness allows obtaining relatively high initial PAM utilization (~ 65% @ 5.6 mA.g<sub>PAM</sub><sup>-1</sup> or 20h discharge rate) using only SnO<sub>2</sub> coating (i.e. without the use of electroplated PbO<sub>2</sub> working as an artificial corrosion layer). However, the cycling of these electrodes with high and moderate depth of discharge profiles showed relatively rapid decay of PAM utilization without considerable increase of the electrode impedance.

The use of phosphoric acid as an electrolyte additive can be a possible route for improvement of the positive electrode capacity retention. According to Voss [16], the phosphoric acid addition in the paste or in the electrolyte of already formed battery, improves the positive plate cycle life, but decrease slightly the PAM utilization. The gelling of the phosphoric acid containing electrolyte with colloid or fumed silica yields further synergy effect of cycle life improvement, and this effect is widely used in the gel-electrolyte Valve-Regulated Lead-Acid Batteries (VRLAB) manufacturing [17]. In contrast, the only source of information about the impact of the phosphoric acid on the positive plate formation process and the cycling beyond it has been found in the doctoral thesis of Gwyneth Morris carried out the Loughborough University three decades ago [18]. The results from this study demonstrated that there is a phosphoric acid concentration threshold of 1% (considering 1.28 s.g. H<sub>2</sub>SO<sub>4</sub> jar formation electrolyte), above which an inhibition of the formation process starts (i.e. impeded electrochemical transformation of lead sulfate and basic lead sulfates into PbO<sub>2</sub>).

The recent attempts to improve the capacity retention of thin-plate titanium supported PbO<sub>2</sub> electrodes using phosphoric acid confirmed the above-mentioned phosphoric acid concentration threshold of 1% [19]. However, the same study showed also that the jar formation in more diluted H<sub>2</sub>SO<sub>4</sub> (for example 1.15 s.g. or 2.5 mol.l<sup>-1</sup>) in the presence of 1% H<sub>3</sub>PO<sub>4</sub> leads also to joint improvement of the PAM utilization and capacity retention on cycling. The aim of the present work is a further investigation of this new effect of the phosphoric acid on the lead dioxide electrochemistry in the context of the bipolar lead-acid battery technology development. In order to get a better insight about the mechanism of interaction between the phosphoric acid and the lead dioxide electrode, the impact of two more different phosphate derivatives has been studied as well. The CaHPO<sub>4</sub> has been selected as an inorganic precursor of H<sub>3</sub>PO<sub>4</sub>, while the poly-vinylphosphonic acid (PVPA) has been chosen as organic polymer analog of the phosphoric acid with potential binder effect [20, 21].

## Experimental

The titanium-supported lead dioxide electrodes have been prepared using SnO<sub>2</sub>-coated titanium foil (grade 1) with a thickness of 250μm embedded in 3D printed grid-like structures presented in the supplementary information (S1). The surface treatment of the titanium has been carried out using rapid dip coating process [22]. The assembled current collectors are pasted with 3BS pastes with the compositions listed in Table 1, prepared with 50%(wt.) sulfuric acid (specific gravity equal to 1.4 g.cm<sup>-3</sup>). Fumed silica (f-SiO<sub>2</sub> purchased from Sigma-Aldrich) was used a paste additive. During the hand-pasting process, the openings of the 3D printed grid-like structure are filled with paste up to the edge using a spatula, resulting in a paste layer with a thickness of 1mm and 2mm (supplementary information S2). The pasted surface of the electrode is further covered by pasting paper (DYNAGRID 328 NG, provided by Glatfelter) and left at room temperature and humidity for 16h for curing. The

electrodes drying is carried out for 24h at 60°C. The weight difference between the “empty” electrode and the dried pasted electrode, excluding the weight of the pasting paper is used to calculate the theoretical capacity, the active material utilization rates and the surface loading of current collector with active material denoted as “ $\gamma$ -coefficient” [23-25]. The cells are assembled using conventional negative plates cut to match the entire size of the positive electrodes, AGM separator (two or three stacked sheets, 220g.m<sup>2</sup>, 1.3mm @ 10kPa provided by Bernard Dumas) and polyethylene envelops allowing the application of external compression. The positive electrode potential has been monitored using Ag/Ag<sub>2</sub>SO<sub>4</sub> reference electrodes filled with 4.5M H<sub>2</sub>SO<sub>4</sub>. The cells are vacuum-assisted filled with 1.15 s.g. H<sub>2</sub>SO<sub>4</sub> (with or without an addition of 1 % wt. of H<sub>3</sub>PO<sub>4</sub>) and jar-formed applying 90h long multistep program which injects 229 % of the nominal capacity of the electrode, accounting 50 % utilization of the theoretical PbO<sub>2</sub> electrochemical equivalent.

The formed cells have been subjected to 20 cycles with 20 h – rated discharge current (5.6 mA.g<sub>PAM</sub><sup>-1</sup>) and a depth of discharge (DoD) equal to 100 %. The charge process has been carried out using constant current / constant voltage sequence starting with a current density of 28 mA.g<sub>PAM</sub><sup>-1</sup> and limiting the voltage to 2.35 V. The constant voltage was maintained for a period of 10 h. The initial cycling was followed by a series of cycles with various discharge current density. The cells have been subjected to periodic electrochemical impedance spectroscopy measurements in two-electrode and three-electrode mode at open circuit voltage (or potential) at least one hour after the termination of the complete charge.

After the completion of the electrochemical characterization, the cells have been subjected to cycling ageing with fixed DoD corresponding to PAM utilization equal to 15% and current density equal to 22.4 mA.g<sub>PAM</sub><sup>-1</sup>. X-ray diffraction (XRD) and scanning electron microscopy (SEM) have been used to characterize the PAM composition and structure after the ageing test.

**Table 1.** Paste compositions and nominal parameters of the studied titanium-supported electrodes.

Cell reference	Positive paste “dry” components					$\gamma$ coefficient	Electrolyte	Nominal capacity
	PbO	H <sub>2</sub> SO <sub>4</sub>	f-SiO <sub>2</sub>	CaHPO <sub>4</sub>	PVPA			
	[%]	[%]	[%]	[%]	[%]		[%]	
B1	92.6	5.1	2.3	---	---	0.63	---	723
<b>B10</b>	92.6	5.1	2.3	---	---	0.77	1	878
B2	90.1	5.0	2.3	2.7	---	0.70	---	806
<b>B5</b>	90.1	5.0	2.3	2.7	---	0.70	1	798
B4	90.6	5.0	2.3	---	2.2	0.61	---	694
<b>B3</b>	90.6	5.0	2.3	---	2.2	0.57	1	658
OB	92.6	5.1	2.3	---	---	0.45	---	517
<b>OO</b>	92.6	5.1	2.3	---	---	0.43	1	498
O7	90.1	5.0	2.3	2.7	---	0.41	---	472
<b>OD</b>	90.1	5.0	2.3	2.7	---	0.41	1	474
<b>OI</b>	94.8	5.2	---	---	---	0.47	1	534
<b>OF</b>	91.0	5.0	0.6	1.7	1.7	0.35	1	399

## Results and discussion

### *Initial performance of the titanium-supported lead dioxide electrodes*

Figure 1 presents the evolution of the discharge capacity of three pairs of cells employing different types of pastes applied with 2 mm thickness. The positive electrodes of each pair of cells have been pasted from the same paste batch and filled with 1.15 s.g. H<sub>2</sub>SO<sub>4</sub> with or without an addition of 1 % wt. of H<sub>3</sub>PO<sub>4</sub>. Figure 1a presents the case where no phosphate derivatives have been added to PAM. It can be seen that the initial capacity is rather poor, however it increases rapidly along the initial cycling. This type of electrochemical behavior can be attributed to the completion of the formation process and the corresponding porous structure development [23]. The effect of the H<sub>3</sub>PO<sub>4</sub> addition to the jar-formation electrolyte is manifested as an active material utilization shift, which is kept approximately the same except in the case of a discharge process with 40h-rated current. The PAM activation effect caused by the presence of H<sub>3</sub>PO<sub>4</sub> in the jar-formation electrolyte repeats with considerable stronger “contrast” at the two other types of positive electrodes (Fig. 1b and 1c). The addition of CaHPO<sub>4</sub> to the paste results in faster initial capacity development followed by faster loss of capacity. When an electrode prepared with same paste is formed in the present of H<sub>3</sub>PO<sub>4</sub> the capacity increase is even faster and PbO<sub>2</sub> utilization becomes higher without an indication for initial capacity fade. This result suggest a synergy effect between the phosphate doping throughout the electrolyte and the paste composition. The adding of PVPA to the paste exerts similar effects, with even stronger synergy due to the inhibition effects of the PVPA when the additive is used all alone, and the further increase of the PAM utilization (going above 60% at 20h-rated discharge regime) when the electrode is formed in the electrolyte containing H<sub>3</sub>PO<sub>4</sub>.

The activation process caused by the addition of the H<sub>3</sub>PO<sub>4</sub> in the jar formation electrolyte have been observed also during the initial cycling of electrodes with 1mm thick active material layer (Fig. 2). The decrease of the electrode thickness results in slightly higher initial capacity values due to enhanced formation process. The further capacity gain at low discharge rates is rather small at the electrodes formed in H<sub>3</sub>PO<sub>4</sub>-free electrolyte. In contrast, the electrodes formed and operating in electrolyte containing H<sub>3</sub>PO<sub>4</sub> developed much higher capacity in faster pace. It can be also seen that all four electrodes with different paste compositions show very similar performance in terms of discharge capacity, all exceeding 140 mAh.g<sub>PAM</sub><sup>-1</sup> or 62% of lead dioxide utilization. This result indicates that the magnitude of the activation effect at the thinner electrodes is more significant, than those of the selected PAM additives. The existence of link between the activation effect and the process of diffusion of the electrolyte species in the pores of the positive electrode can be suggested too.

The activation effect can be further visualized and analyzed by the relationship between the electrodes capacity and the discharge current density. Figure 3 presents the corresponding plots taking into account the maximum PAM utilization values from the data shown in Figure 1 and 2. It can be seen that the jar-formation in the presence of H<sub>3</sub>PO<sub>4</sub> practically “shifts” the electrode capacity towards higher values in the whole studied current density range. The only exception was the 40h-rated discharge of cell “B1” (Fig. 3a). The capacity gain (i.e. the magnitude of the activation effect) varies from case to case, mostly remaining in the range of 40 – 50 mAh.g<sub>PAM</sub><sup>-1</sup>. This suggests considerable difference created in the PAM structure during the formation and the initial cycling, i.e. after the paste mixing and curing which are considered as principal processes forming the PAM morphology and the corresponding electrochemical performance [23].

The data were analyzed further using the Peukert equation:

$$t_{dsch} = K \cdot I_{dsch}^{-n}$$

where  $t_{dsch}$  is the discharge duration (in minutes),  $I_{dsch}$  is the discharge current (in  $\text{mA}\cdot\text{g}_{\text{PAM}}^{-1}$ ), and  $n$  and  $K$  are empiric coefficients related to the high-rate capacity ( $n$ ) and the overall active material utilization ( $K$ ). The obtained values of  $n$  and  $K$  are listed in Table 2. The calculated data-fits are presented graphically in Figure 3 as dotted lines. It can be seen that all experimental data correlate rather well with the Peukert equation, especially at higher discharge rates. This summary of the experimental results allows one more analytical appraisal of the activation effect of the phosphoric acid. From one hand in every studied case there is a decrease of the coefficient “ $n$ ”, which is associated with improved high rate discharge capacity. From the other, the increase of the coefficient “ $K$ ” indicates improved global PAM utilization. The effects from the decrease of the electrode thickness are also similar, indicating the vital role of the electrolyte species diffusion in the discharge process.

**Table 2.** Summary of the discharge data fitting using the Peukert equation.

Cell reference	Paste type	PAM thickness	H <sub>3</sub> PO <sub>4</sub> added to the electrolyte	Peukert coefficient “ $n$ ”	Peukert coefficient “ $K$ ”
B1	Phosphate-free	2 mm	No	1.338	9315
<b>B10</b>	<b>Phosphate-free</b>	<b>2 mm</b>	<b>Yes</b>	<b>1.210</b>	<b>9692</b>
B2	PAM with CaHPO <sub>4</sub>	2 mm	No	1.360	8278
<b>B5</b>	<b>PAM with CaHPO<sub>4</sub></b>	<b>2 mm</b>	<b>Yes</b>	<b>1.246</b>	<b>11800</b>
B4	PAM with PVPA	2 mm	No	1.393	7954
<b>B3</b>	<b>PAM with PVPA</b>	<b>2 mm</b>	<b>Yes</b>	<b>1.248</b>	<b>13192</b>
OB	Phosphate-free	1 mm	No	1.278	8989
<b>OO</b>	<b>Phosphate-free</b>	<b>1 mm</b>	<b>Yes</b>	<b>1.213</b>	<b>11984</b>
O7	PAM with CaHPO <sub>4</sub>	1 mm	No	1.317	7903
<b>OD</b>	<b>PAM with CaHPO<sub>4</sub></b>	<b>1 mm</b>	<b>Yes</b>	<b>1.185</b>	<b>11259</b>
<b>OI</b>	<b>CaHPO<sub>4</sub> + PVPA</b>	<b>1 mm</b>	<b>Yes</b>	<b>1.253</b>	<b>12531</b>
<b>OF</b>	<b>Additives-free</b>	<b>1 mm</b>	<b>Yes</b>	<b>1.255</b>	<b>11923</b>

The mechanism of the activation process can be tracked down further by the analysis of the voltage and current transients during the initial cycling (i.e. Peukert test series). Figure 4 presents the corresponding test cycles with 2h – rated discharge current ( $56 \text{ mA}\cdot\text{g}_{\text{PAM}}^{-1}$ ) for the case of 2mm – thick electrodes with three different PAM compositions. The comparison of the discharge voltage transients from Figure 4a, 4d and 4g shows that the addition of H<sub>3</sub>PO<sub>4</sub> in the electrolyte shifts the voltage plateau to higher values. The observed effect is in good agreement with literature [16] and the analysis of the positive half-cell potential allowed relating it entirely to the positive electrode (supplementary information S3). It can be also denoted that the PAM doping with inorganic or organic species containing phosphates alone (i.e. in pristine H<sub>2</sub>SO<sub>4</sub> electrolyte) also shifts the electrode potential to higher values. The comparison of the discharge duration at this regime demonstrates well the magnitude of the activation effect – at this discharge rate the capacity gains are considerable. The comparison of the voltage and current transients during the subsequent recharge shows that the electrolyte doping with H<sub>3</sub>PO<sub>4</sub> and the PAM doping with phosphate additives results in significant differences in the electrode kinetics. In pristine H<sub>2</sub>SO<sub>4</sub> electrolyte, the charge process starts with a spike in the positive plate potential denoted often as “charge coup de fouet”. In the case of state of the art lead-acid batteries, according to Pavlov et al., the effect can be related to the electrochemical oxidation of non-stoichiometric lead oxides (PbO<sub>n</sub>) formed at the interface between the active material and the current collector [24]. It has been observed also during the cycling of thin-plate Ti-supported electrodes [15] as well as at the carbon - supported lead –

methanesulfonic acid redox-flow cells [26]. The voltage plots in Figure 4e and 4h show that the PAM phosphate doping alone enhances the formation of  $PbO_n$  significantly due to the increase of the voltage spike intensity. It is also rather consistent with the observed lower discharge capacity values. In contrast, when the electrodes are formed in  $H_3PO_4$  doped electrolytes, the charge process starts with a progressive increase of the cell voltage (i.e. there is no voltage spike), no matter what is the PAM composition. This result is an indication that the lead dioxide structure and morphology formed in the presence of  $H_3PO_4$  enhance the electrochemical and chemical transformation of intermediate compounds (such as non-stoichiometric lead oxides and hydroxides) formed during the positive electrode discharge. Apart from its initial stage, the charge process at all six cells proceeds without any major qualitative difference – the voltage increases progressively reaching the selected limit of 2.35V. Beyond this point, the charge is carried out in constant voltage mode, during which the current decreases due to the decreasing content of  $PbSO_4$  in the electrodes.

The voltage and current transients during the 2h-rated discharge tests of 1 mm thick electrodes are plotted in Figure 5. It can be seen that decrease of the PAM thickness improves moderately the discharge performance of the cells without phosphoric doping of the active material (Fig. 5a, 5b and 5c). **There are no qualitative changes of voltage and current evolution pattern indicating that the mechanism of the electrochemical processes remains the same.** In both cases the discharge duration gains are in the range of 0.2 h (i.e. in the range of 10% considering the nominal discharge rate of 2h). The voltage gap between the cells formed without and with  $H_3PO_4$  addition to the electrolyte remains similar, yet smaller due to lower voltage drop associated with the thinner positive electrode and the thinner AGM separator (2 stacked layers of AGM in this case vs. 3 layers used in the cells with thicker PAM). The charge process starts in the same way without any voltage spike when the electrolyte contains 1%  $H_3PO_4$  and *vice versa*, indicating that the decreased PAM thickness also does not change the discharge mechanism significantly. The same type of trends can be seen in the electrochemical behavior of the cells employing paste doped with  $CaHPO_4$  shown in Figures 5d, 5e and 5f. In this case, the decrease of the PAM thickness improves only the performance of the cell containing  $H_3PO_4$  added to the electrolyte. Again, the poor discharge performance of the other cell correlates with the appearance of more intense initial charge voltage spike indicating that the effect of the  $CaHPO_4$  on the  $PbO_2$  electrochemistry is inhibitive when the additive is used in  $H_3PO_4$ -free electrolyte. The current and voltage transients of other two cells with different PAM compositions formed in electrolytes containing 1%  $H_3PO_4$  are presented in Figure 5g, 5h and 5i. The obtained data repeat rather well the results observed at the other cells employing the same electrolyte. This observation confirms further the suggestion that the magnitude of the activation caused by the doped electrolyte is much higher than those caused by the phosphate-containing compounds introduced in the electrodes during the positive paste mixing. **It can be also concluded that impact of the electrolyte diffusion process “tuned” via the electrode or the active material thickness should be considered as an additional degree of freedom to be taken into account during the optimization of the paste and the electrolyte composition.**

#### *Cycling aging tests*

The selected cycling ageing protocol applied during this study was comprised of 1.5h long discharge period corresponding to 15% PAM utilization preceded and followed by 5min long rest periods and CC/CV charge. The charge and discharge current density was fixed to  $22.4 \text{ mA} \cdot \text{g}_{\text{PAM}}^{-1}$ . The voltage during the CV phase was fixed to 2.35 V for the cells doped with phosphorus additives and the duration was adjusted to deliver a ratio between the charge and discharge quantity (often denoted also as “charge factor”) staying in the range of 102 – 105%. Several check-up cycles with 20h-rated

discharge current and 100% DOD were carried out each 500 shallow cycles in order to track down the evolution of the PAM utilization, which represents the electrochemical activity of PbO<sub>2</sub>. The impedance spectra of the cell and the positive electrode have been measured after the check-up cycles as well at a state of charge equal to 100%.

The results from the ageing of the pair of cells with 2 mm thick PAM without phosphorus dopants are shown in Figure 6. The first parameter tracking down the progress of the electrode ageing is the end of discharge (EOD) voltage point. It is plotted in Figure 6a and the data match precisely the evolution of positive electrode potential in the end of the discharge due to the oversized capacity of the negative counter-electrode. It can be seen that the EOD voltage of both cells remains rather stable during the first 500 cycles set. This is a good indication that the applied charge conditions exert a fair balance between the overcharge and the lead sulfate build up in PAM. During the second cycling set both cells experience loss of performance expressed as a progressive decay of the EOD, marking the end of lifetime of the positive electrodes. The comparison of the evolution of the 20h-rated capacity measured periodically is shown in Figure 6b. It can be seen that the ageing of this pair of cells follows different patterns. The cell B1 which operates without H<sub>3</sub>PO<sub>4</sub> added to the electrolyte experiences about 10% decrease of PAM utilization after 500 shallow cycles and less than 1% further decrease beyond this point. The periodic measurement of the cell and positive electrode impedance shows almost negligible increase of the ohmic resistance (Fig. 6c). The latter is a good indication that the capacity loss along the aging is not related a degradation of the Ti/SnO<sub>2</sub> current collector. The evolution of the PAM utilization in the cell B10 matches well a linear decrease of the capacity with the number of cycles (Fig. 6b). The experimental data shown in Figure 6d indicate that the aging of this cell proceeds with slightly higher increase of the positive electrode impedance.

The analysis of the cell voltage and current transients during the check-up in the end of the cycling of cells B1 and B10 allows getting more insights about the ageing mechanism. The comparison of the voltage data during the discharge with 5.6 mA.g<sup>-1</sup> (C/20h discharge rate) presented in Figure 7a and 7d shows that the voltage shift related to the addition of the H<sub>3</sub>PO<sub>4</sub> remains almost the same (about 0.1V). There is no qualitative changes neither in the shape of the discharge transients in comparison with the data observed during the initial cycling. On the other hand, one can see that the presence of H<sub>3</sub>PO<sub>4</sub> induces a significant change in the charge behavior of cell B10 in the end of the cycle ageing. The charge process begins with a very intense voltage peak with relatively long duration (the charge sequence includes an initial short galvanostatic step without a voltage limit in order to allow the “appearance” of the charge “coup de fouet” effect). The coulometric equivalent of the peak is 12.4 mAh.g<sup>-1</sup>, which corresponds to 5.5% of the total PbO<sub>2</sub> content. On the other hand, the duration of the voltage spike observed at the cell B1, which does not contain any kind of phosphate doping is in the range of 20 s, corresponding to about 0.01% of the total PbO<sub>2</sub> content.

Such result indicates that the discharge reaction in the presence of H<sub>3</sub>PO<sub>4</sub> produces significant quantity of Pb(II) compounds with high ohmic resistance, which should be different from the PbSO<sub>4</sub> formed during the discharge of the “fresh” electrodes. The slight increase of electrode impedance in fully charged state, observed in Figure 6d, suggests that small fraction of these resistive discharge reaction products remains unaltered after the recharge and thus accumulates cycle by cycle.

Figure 8 summarizes the impact of the PVPA added to the PAM on the electrode ageing. In the case of H<sub>3</sub>PO<sub>4</sub>-free electrolyte, the electrode degrades very rapidly and the EOD voltage drops within 100 shallow cycles. In contrast, the electrode operating in H<sub>3</sub>PO<sub>4</sub> – doped electrolyte reaches the EOD voltage limit after nearly 500 cycles (Fig. 8a). The data in Figure 8b show that the ageing of the “activated” electrode in cell B3 takes place with considerable loss of PAM utilization, which dropped three times from 63 to 21%. The periodic measurements of the impedance of this pair of cells shows

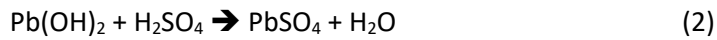
relatively small increase of the overall positive electrode resistance, indicating that the “capacitive” ageing is predominant, while any possible degradation related to the current collector degradation is rather small. The cycling of the cell B4 proceeds without increase of the ohmic resistance, but with a considerable growth of the medium-frequency impedance loop often related to the charge transfer phenomenon. In contrast, the ageing of the other cell B3 proceeds with simultaneous increase of the high and medium frequency impedance. It can be seen also that the later features a broad depressed part which can be associated with the presence of several time-constants. Such type of results indicates the appearance of different phenomena impeding the transfer of charges in the porous PbO<sub>2</sub> active material, for example the adoption of H<sub>3</sub>PO<sub>4</sub>, H<sub>2</sub>PO<sub>4</sub><sup>-</sup> or other phosphate species [27].

The compression of the cell B3 was readjusted after the 20h-rated capacity test in order to evaluate the possibility of PAM softening as a potential mechanism reducing the PAM utilization. The impact of this measure can be seen first in Figure 8b as a jump of the PAM utilization from 20 to 34%. Despite this significant discharge performance gain, it can be seen that the loss of contact between the PAM particles during the cycling cannot explain the major part of the capacity loss. Moreover, the gain achieved by the compression readjustment is relatively short-lasting.

The effects from the compression readjustment can be tracked down further by the analysis of the voltage and current transients during the check-up cycles in the end of the cells’ cycle life presented in Figure 9. The electrochemical discharge behavior of the cell B4 (without H<sub>3</sub>PO<sub>4</sub>), plotted in Figure 9a is rather similar to the previous case shown in Figure 7a. The voltage plateau is well above 2V and the end of the discharge voltage “knee” can be easily distinguished. This result is fairly consistent with the small increase of the cell impedance observed in Figure 8c. The discharge behavior of the cell B3 formed and cycled in presence of H<sub>3</sub>PO<sub>4</sub> (Fig. 9d) features two distinct differences from its counterpart (cell B4). First, the discharge voltage plateau is shifted lower, thus being in good agreement with the observed increase of the impedance (Fig. 8d), and second, an inflection point in the discharge voltage “knee” region of the transient, which indicates the occurrence of a solid-state electrochemical process related to the formation of resistive non-stoichiometric PbO<sub>n</sub>, with n < 1.5 [23, 24].

The impact of the compression readjustment on the discharge process can be seen in Figure 9d. The voltage plateau shifts to higher values due to the restored electric contacts between the PbO<sub>2</sub> particles and capacity improves. In the same time the inflection point in the discharge voltage “knee” region becomes more pronounced, i.e. more PbO<sub>n</sub> should be formed. The analysis of the charge data also indicates that the addition of PVPA enhances the formation and accumulation of resistive PbO<sub>n</sub> discharge products. When the cell does not contain any H<sub>3</sub>PO<sub>4</sub> their quantity remains relatively small (about 1.25% of the total PbO<sub>2</sub> content can be considered as resistive PbO<sub>n</sub> transformed during the charge voltage peak duration), most probably due to the small number of cycles achieved by the cell B4. On the hand, the recharge of the cell B3 operating with H<sub>3</sub>PO<sub>4</sub> doped electrolyte proceeds with more intense initial voltage peak with a duration exceeding 20 min (> 4.2% of the total PbO<sub>2</sub> equivalent in the electrode). The increase of the cell stack compression intensifies additionally the latter phenomenon indicating that more PbO<sub>n</sub> is formed at higher compression. Since the increased stack compression should squeeze out part of the electrolyte from the PAM and AGM pores, we can suggest that the formation of PbO<sub>n</sub> is linked with the impeded H<sub>2</sub>SO<sub>4</sub> transport to the electrochemical reaction sites. In contrast, the access of H<sup>+</sup> ions will not be impacted so much by the compression due to their smaller size, increased mobility and hydrated nature of the PbO<sub>2</sub> surface [28]. Thus, if the PbO<sub>2</sub> discharge reaction mechanism [29] is simplified to a two-step process:





one can suppose that the presence of the phosphate additives ( $\text{H}_3\text{PO}_4$  and PVPA) and the impeded net transport of  $\text{H}_2\text{SO}_4$  species are both slowing down the Reaction (2), the first by an adsorption and the second by a pore size squeezing process. Since the  $\text{Pb(OH)}_2$  is not stable [30], it is further transformed into hydrated non-stoichiometric lead oxides, possible throughout a solid-state reaction with the non-reacted  $\text{PbO}_2$  nearby.

Figure 10 presents the summary of the ageing test results of three cells employing positive paste containing  $\text{CaHPO}_4$ . The cell B2 formed without  $\text{H}_3\text{PO}_4$  in the electrolyte fails after 200 shallow cycles, while its counterpart cell B5, formed and operating with  $\text{H}_3\text{PO}_4$  doped electrolyte reaches the set end-of-life criterion after nearly 1000 cycles. The comparison of these data with the previous case (PVPA-doped PAM) shows that the formation and cycling in the electrolyte containing  $\text{H}_3\text{PO}_4$  increases the cycle-life roughly 5 times. The periodic measurement of the impedance showed also rather similar trends: the high- and medium-frequency impedance of cell B2 does not change significantly after the 200 cycles, while the impedance of the cell B5 shifts due to an increase of the positive electrode ohmic resistance.

The results in Figure 10 show further that the decrease of the PAM thickness impacts very strongly the aging process of the electrodes formed and operating in electrolyte containing  $\text{H}_3\text{PO}_4$ . The performance of the cell OD employing 1 mm thick PAM layer achieved more than 1500 cycles. The evolution of the 20h-capacity and the electrode impedance show that the degradation is almost purely capacitive and it is much less impacted by the compression readjustment applied after the first end of discharge voltage drop. This result confirms further how the loss of performance of the  $\text{PbO}_2$  on cycling is linked with  $\text{H}_2\text{SO}_4$  species diffusion process – the faster diffusion will enhance the chemical reaction (2), thus less  $\text{PbO}_n$  will be formed (thus explaining the negligible increase of the impedance as well).

The analysis of the discharge voltage transients in the end of the cells' lifetime presented in Figure 11a and 11d shows good correlation with the impedance data plotted in Figure 10 c, 10d and 10e. The voltage plateaus of the cells B2 and OD do not differ much from those observed at their initial state, while there is a visible voltage drop at the cell B5 correlating well with the increased impedance. The formation of resistive  $\text{PbO}_n$  species during the discharge process is visible at all three cells as a voltage peak in the beginning of the charge, however the severity of this phenomenon is markedly slower when  $\text{CaHPO}_4$  is used as an additive, even after the compression readjustment. These results suggest the existence of synergy effect between the uses of  $\text{CaHPO}_4$  as a PAM additive and the  $\text{H}_3\text{PO}_4$  as a jar formation electrolyte additive. It should be also denoted that shortly after the application of the compression readjustment of the cells B5 and OD internal micro-short circuits appeared. The latter were detected due to the increased end of charge steady-state current (Fig. 11f) and the elevated charge factor values at the very end of the cycling (Fig. 10a). Such type of problem and failure mode are rather related to the battery separator materials and will not be discussed in the present work in more details [31].

#### *Teardown analysis and PAM characterization*

The electrochemical studies discussed in the previous paragraphs were followed by complete recharge and teardown analysis including visual evaluation of the cells components (positive and negative electrodes, AGM separator, and electrolyte density measurements), X-ray diffraction measurements and scanning electron microscopy observations. The two characterization methods

were applied only on the positive electrodes after a consecutive washing with tap and deionized water and an overnight drying in air at 60°C.

PAM samples from seven of the cells have been analyzed using powder XRD analysis (B5, OD, B8, B3, B4, B1 and B10). All results from these measurements showed that over 99% of the PAM crystallographic composition is comprised of  $\beta$ -PbO<sub>2</sub>, which is in good agreement with the recent results obtained on titanium-supported thin-plate electrodes [15]. Figure 12 presents a comparison of four PAM samples from cells B1, B5, B10 and OD. It can be seen that the XRD peaks of the PAM from the cell B1, which does not contain any kind of phosphate additives, are much higher and more narrow (the measurements were carried out in a single day on the same equipment without and changes in the system setup). This is a good indication that the PbO<sub>2</sub> particles in this cell are larger and possess higher crystallinity in comparison with the other cells which have been formed and cycled in electrolyte containing H<sub>3</sub>PO<sub>4</sub>. A closer inspection of the data revealed the presence of traces of  $\alpha$ -PbO<sub>2</sub> in the cells B5 and B10, both below 1% of volume, while in the other two cases the crystallographic purity of the  $\beta$ -PbO<sub>2</sub> was practically equal to 100%.

Figure 13 presents scanning electron micrographs (SEM) of PAM samples from the cells OD, B5 and B1, all taken from mid-thickness of the pallets' cross-section. The PbO<sub>2</sub> morphology in the samples B5 and OD (both prepared from the same paste batch and formed and cycled in H<sub>3</sub>PO<sub>4</sub> doped electrolyte) is very similar. The vast majority of the particles' size is below 100 nm. In contrast, the sample from the cell B1 contains micron-sized PbO<sub>2</sub> crystals with fairly defined plain surfaces and edges. These results are in very good agreement with the XRD data, demonstrating that the use of H<sub>3</sub>PO<sub>4</sub>-doped electrolyte during the formation and cycling suppresses the PbO<sub>2</sub> crystal growth in relatively long-term period. In consequence, the smaller PAM particle size explains the higher capacity values, especially those obtained during high-rate discharge experiments.

The visual observations of the electrodes in the end of the long-term cycling allows getting at least a partial explanation of the capacity fade mechanism. Figure 14a presents a close look photo of the positive electrode from cell OD during the removal of the PAM pallets for the above-mentioned XRD and SEM analysis. It was found that the 3D printed ABS plastic and the titanium current collector were practically intact, while the surface of the PAM pallets facing the AGM separator took a concave shape due to the stack compression action (schematically illustrated in Fig. 14b). The synthetic part of the pasting paper has been distinguished as well, being stuck on the concave surface of the PAM, as well as on the 3D printed grid. The inspection of the adjacent AGM material showed that considerable amount of PAM particles passed across the pasting paper and entered the separator pores due to the combined action of the softening process and the applied compression. The AGM zone infused with PAM particles has been also analyzed with X-ray diffraction. The results presented in Figure 14c show that about 95% of the crystallographic phases in the studied sample are comprised from  $\beta$ -PbO<sub>2</sub> with lower peak intensity and broader peak half-width in comparison with the data shown in Figure 12. The same type of results has been found in the other analyzed AGM sample facing the positive electrode in the cell B3. These data indicate that smaller PbO<sub>2</sub> particles are "squeezed" out the electrode and forced inside the larger AGM pores located in the z-direction of the separator plane during the cycling. One can suppose that this fraction of the PbO<sub>2</sub> would be much less reactive during the discharge process, in a way similar to the PbO<sub>2</sub> denoted as "softened" PAM [7]. The presence of fine PbO<sub>2</sub> particles in the AGM pores could have also a "pore-clogging" effect which is another type of capacity-limiting phenomenon cutting the electrolyte transport from the bulk of the separator to the positive electrode inner pores. A possible mitigation of these PAM degradation effects could be the use of more rigid porous interface between the PAM and the AGM separator. There are at least two alternatives, which can be found on the lead-acid battery

components market – the porous woven or non-woven tissue used for tubular positive plate gauntlets, or the Hollingsworth & Vose rigid glass-fiber separator material brand Hi-Sep™ which can be used instead of a microporous polyethylene flooded battery separator [32].

The absence of detectable quantities of  $\text{PbSO}_4$  in the tested samples shows that the charge process of thick titanium-supported positive electrodes is not hindered in general. The electrochemical tests showed that the current collectors do not show any indications of significant degradation due to a corrosion or a passivation phenomena (such would appear as systematic increase of the ohmic resistance or growing capacitive loops in the medium-frequency impedance of fully charged cell). The “Agglomerate Of Spheres” (Kugelhaufen) model of PAM structure [33] could be used to explain one of the possible mechanisms of the degradation process which excludes large fraction of the  $\text{PbO}_2$  from the electrode capacity. In this case, one can suppose that the incomplete discharge process leading to the formation of domains rich of resistive  $\text{PbO}_n$  ( $n < 1.5$ ) takes place only at the contact zones between adjacent  $\text{PbO}_2$  nano-particles, leaving no “crystallographic trace”. The latter explains the absence of any crystallographic phases different from  $\text{PbO}_2$  ( $\beta$  and  $\alpha$ ). One can also suggest that at least, part of the capacity loss could be related to slow accumulation of  $\text{PbO}_2$  with very low concentration of defects and rather poor conductivity and electrochemical activity. Such kind of  $\beta$ - $\text{PbO}_2$  with close to ideal stoichiometry has been observed in a recent study using high-definition transmission electrode microscopy observation of titanium supported electrodes with low PAM utilization [15]. Obviously, the estimation of the contribution of each capacity degradation mode (softening/PAM penetration in the AGM, accumulation of resistive  $\text{PbO}_n$  and build-up of resistive  $\text{PbO}_2$  with close to ideal stoichiometry) requires further studies at nano-scale level. It is expected that such methods will be able to reveal also more details about the interaction between the PAM and phosphate species.

## Conclusions

The work presents the study of a recently observed effect of improvement of the electrochemical performance of titanium-supported positive lead-acid battery electrodes. This effect can be summarized as simultaneous increase of the capacity and cycle life when the used electrolyte for jar-formation contains 1% (wt.)  $\text{H}_3\text{PO}_4$  and its density is close to  $1.15 \text{ g.cm}^{-3}$  (prior to the cell filling process). After a structural characterization of the positive active materials, the improvement was attributed to the grain-refining action of the added  $\text{H}_3\text{PO}_4$ . It was also found that there are synergies when different types of phosphate derivatives are jointly introduced in the cell ( $\text{H}_3\text{PO}_4$  added to the electrolyte and phosphate derivatives added to the positive paste). The electrochemical tests carried out on the aged electrodes showed that the loss of performance can be related to three types of PAM degradation mechanisms acting jointly – a PAM softening process, accumulation of resistive non-stoichiometric lead oxides ( $\text{PbO}_n$  with  $n < 1.5$ ) and build-up of highly crystalline  $\text{PbO}_2$  with low defects concentration and low ohmic conductivity. In the same time, the titanium-based current collectors showed no indications of degradation due to a corrosion or a passivation. The combined benefits coming from the use of titanium-based support and the phosphoric acid activation effect can be used to in the development of the next generation bipolar lead-acid batteries offering both long calendar and cycle lifetime.

The beneficial impact of the  $\text{H}_3\text{PO}_4$  addition to the electrolyte for a jar formation process should be studied further in other emerging lead-based storage systems relying on conventional current collector lead alloys, for example AGM-VRLA batteries with thin-plate pure lead electrode technology or hybrid battery-electrolyzer devices combining the energy storage and the hydrogen production

functionalities [34, 35]. The observed decrease of the oxygen overvoltage caused by the presence of the  $\text{H}_3\text{PO}_4$  in the electrolyte can be particularly beneficial for the second type due to the enhanced water electrolysis at the positive electrode resulting in improved power to hydrogen conversion efficiency.

## Acknowledgement

This work has been realized in association with INES.2S within the French national program Investments for the Future (ANR-10-IEED-0014-01) and received funding from the European Union's Horizon Europe research and innovation program under the grant 'Low-Cost, Circular, plug & play, off grid Energy for Remote Locations including Hydrogen' (Project LoCEL-H2 - 101096033).

## References

1. C. Pillot, F. Renard, "The rechargeable battery and main trends 2020-2030", European Lead Battery Conference, 6 – 9 September 2022, Lyon, France
2. J. Garche and P.T. Moseley, "Electrochemical Energy Storage for Renewable Sources and Grid Balancing", Elsevier, Amsterdam, 2015, p. 13
3. EBP, "Economic Contribution of the European Lead Battery Industry", report published online by EUROBAT and the International Lead Association (ILA), available online at: <https://ila-lead.org/resources/>
4. R.D. Prengaman and A.H. Mirza in "Lead-Acid Batteries for Future Automobiles" (eds. J. Garche, E; Karden, P.T. Moseley, D.A.J. Rand), Chapter 20 "Recycling concepts for lead-acid batteries", Elsevier Amsterdam, 2017, p. 575
5. J. Büngeler, E. Cattaneo, B. Riegel, D.U. Sauer, J. Power Sources, **375**, 53 (2018)
6. A. Kirchev, S. Dumenil, M. Alias, A. De Mascarel, M. Perrin, J. Power Sources, **279**, 809 (2015)
7. A. Cooper and P.T. Moseley, J. Power Sources, **113**, 200 (2003)
8. P. Faber, D.H. Collins (Ed.), "Power Sources", vol. 4, Oriel Press, Newcastle upon Tyne (1974), pp. 525-538
9. G. Trasatti, G. Lodi, "Electrodes of Conductive Metallic Oxides", Part B, Elsevier, New York, 1980, p. 592
10. J. Lannelongue, M. Cugnet, N. Guillet, A. Kirchev, J. Power Sources, **352**, 194 (2017)
11. M.J. Donachie, "Titanium: A Technical Guide" (2<sup>nd</sup> ed.), ASM International, Ohio, 2000, p. 123
12. V.L. Grosvenor, N. Pinsky, US Patent 5 800 946, 1 September 1998
13. I. Kurisawa, M. Shiomi, S. Ohsumi, M. Iwata, M. Tsubota, J. Power Sources, **95**, 125 (2001)
14. I. Kurisawa, K. Fujita, M. Shiomi, S. Osumi, K. Matsui, "Study of an advanced VRLA battery with titanium electrode", IEEE 30th International Telecommunications Energy Conference, INTELEC 2009, pp. 1-6

15. J. Lannelongue, M. Cugnet, N. Guillet, E. De Vito, A. Boulineau, A. Kirchev, J. Energy Storage, **20**, 230 (2018)
16. E. Voss, J. Power Sources, **24**, 171 (1988)
17. O. Jache, US Patent 3 765 942, 16 October 1973
18. G. Morris, "The effect of orthophosphoric acid on lead dioxide electrodes", PhD thesis, Loughborough University, December, 1992, p. 93-94
19. J. Lannelongue, A. Kirchev, M. Cugnet, European Patent EP3474352 (A1), 2019-04-24
20. B. Bingöl, "Synthesis and Characterization of Poly(vinylphosphonic acid) for Proton Exchange Membranes in Fuel Cells", PhD thesis, University of Mainz "Johannes Gutenberg", 2007
21. N. Matsumi, N. Takamori, T. Yamazaki, International patent application WO2022/196604 A1
22. A. Kirchev, M. Cugnet, J. Lannelongue, European Patent EP3607107 (A1), 2020-02-12
23. D. Pavlov, S. Ruevski, J. Power Sources, **95**, 191 (2001)
24. D. Pavlov, G. Petkova, M. Dimitrov, M. Shiomi, M. Tsubota, J. Power Sources, **87**, 39 (2000)
25. D. Pavlov, G. Petkova, J. Electrochem. Soc., **145**, A644 (2002)
26. A. Oury, A. Kirchev, Y. Bultel, E. Chainet, Electrochimica Acta, **71**, 140 (2012)
27. J.P. Carr and N.A. Hampson, Chem. Rev., **72**, 679 (1972)
28. D. Pavlov, J. Electrochem. Soc., **139**, 3075 (1992)
29. H. Bode, "Lead-Acid Batteries", Wiley-Interscience, New York, 1977, p. 104
30. W.N. Perera, G. Hefter, and P.M. Sipos, Inorg. Chem., **40**, 3974 (2001)
31. Y. Zeng, J. Hu, W. Ye, W. Zhao, G. Zhou, Y. Guo, J. Power Sources, **286**, 182 (2015)
32. Hi-Sep™ product brochure, Hollingsworth & Vose company website, available at <https://www.hollingsworth-vose.com/brands/energy/hi-sep/>
33. A. Winsel, E. Bashtavelova, J. Power Sources, **73**, 242 (1998)
34. G. Langer, B. Riegel, E. Cattaneo, "Challenges in the Development of high performance long life Lead Acid Batteries", Proceedings of the 11<sup>th</sup> International Conference on Lead-Acid Batteries LABAT'2021, 8-11 June, Virtual conference, p. 81
35. D. Strickland, J.G. Wilson, J. Barton, M. Brenton, "Lead acid battolysers - the pathway to low-cost green hydrogen?", European Lead Battery Conference, 6 – 9 September 2022, Lyon, France

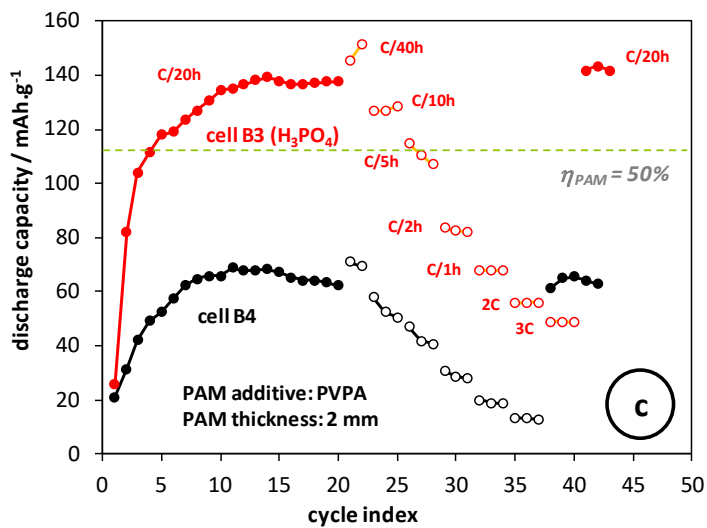
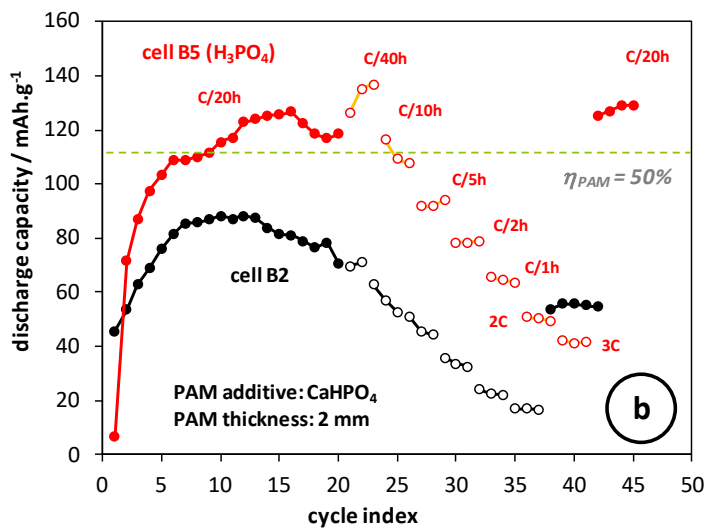
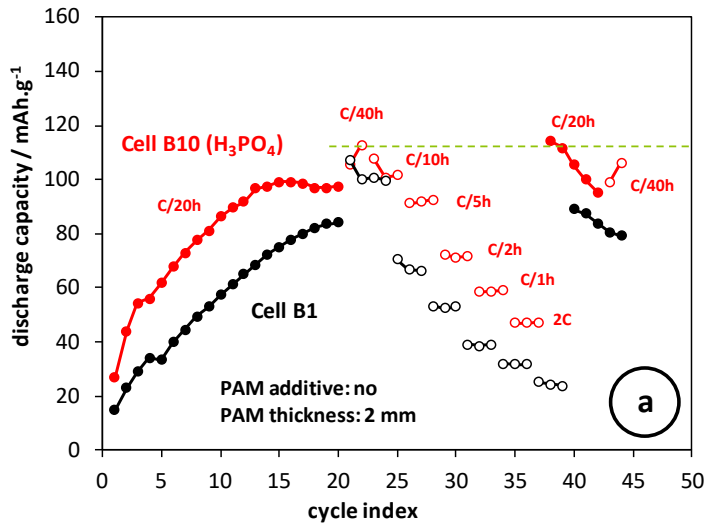


**Fig. 1.** Evolution of the capacity of titanium-supported electrodes with 2 mm thick PAM during the initial cycling tests.

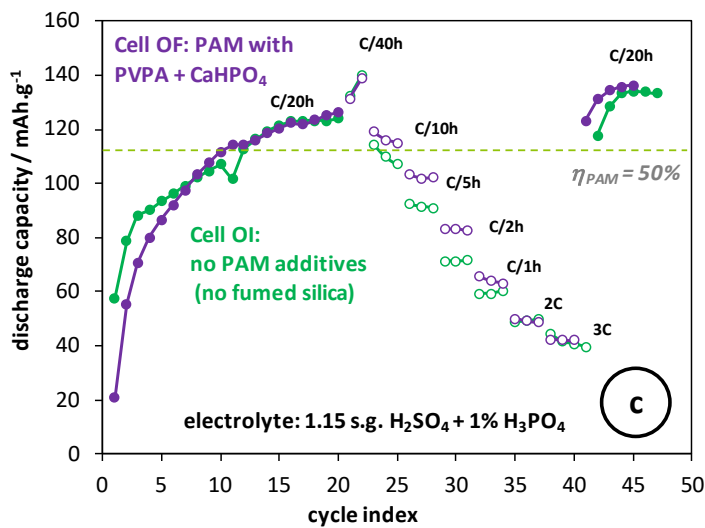
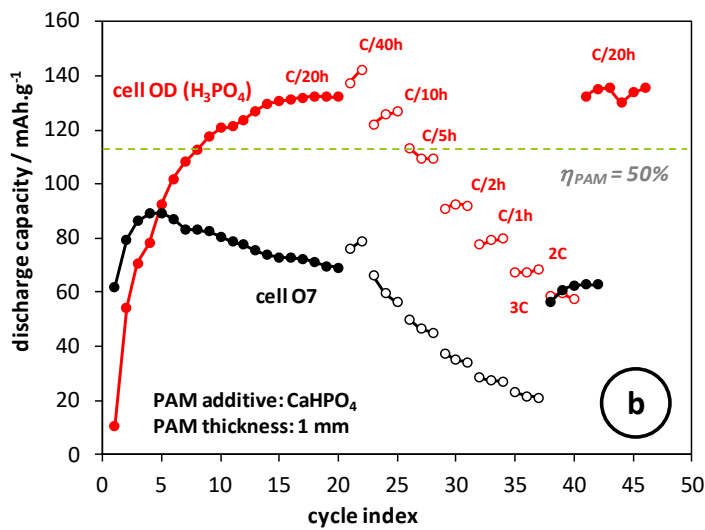
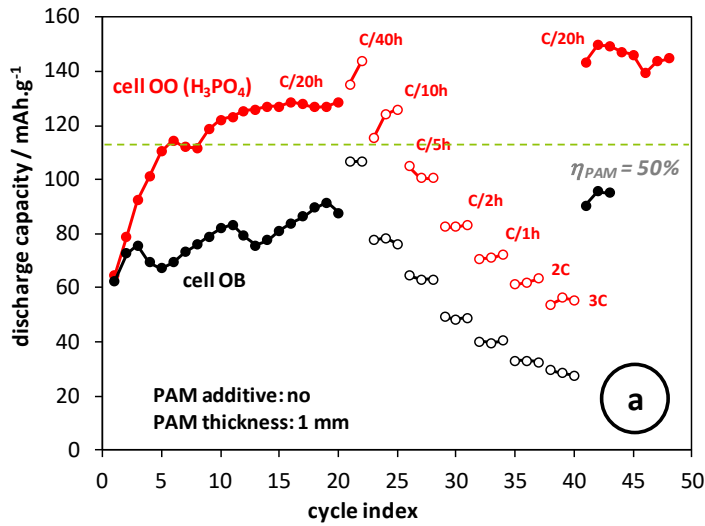


**Fig. 2.** Evolution of the capacity of titanium-supported electrodes with 1 mm thick PAM during the initial cycling tests.

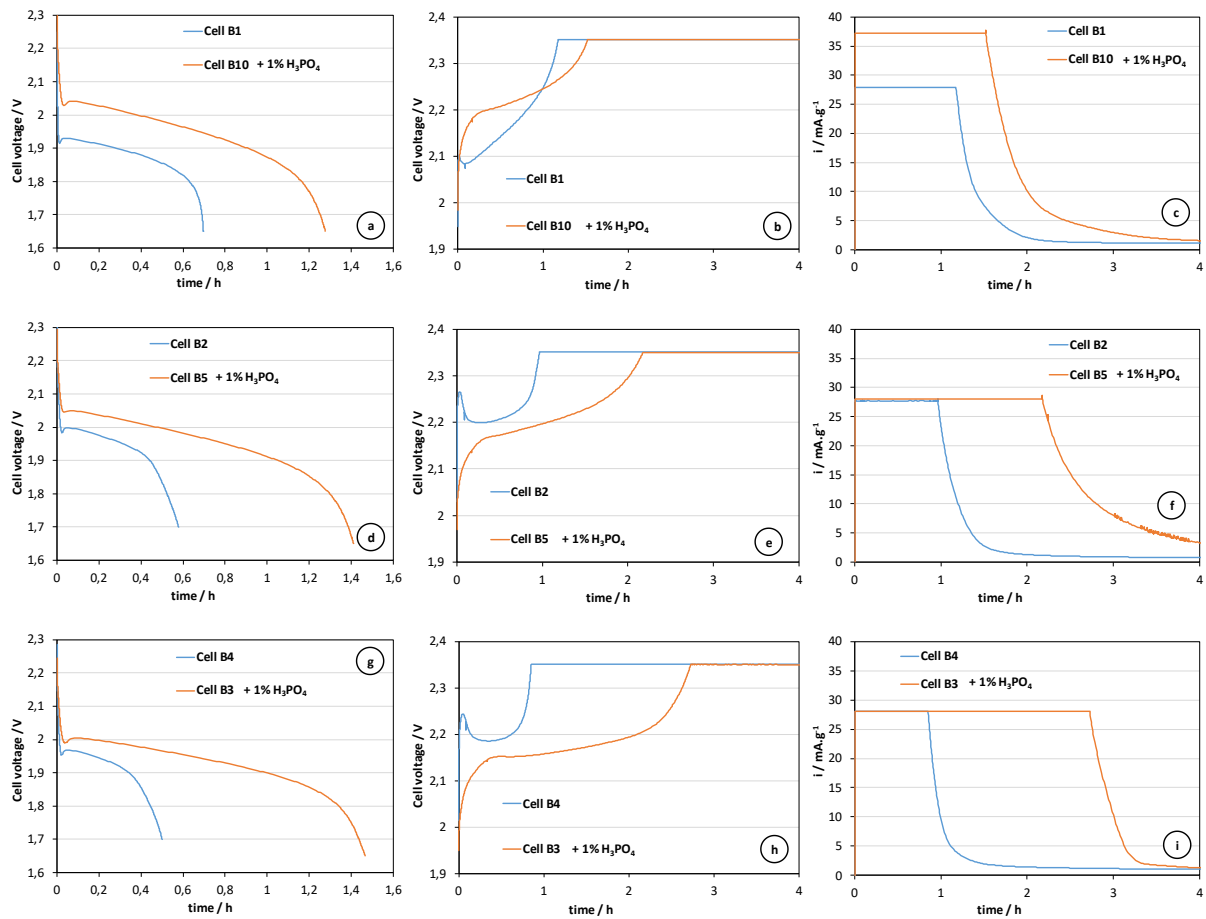


**Fig. 3.** Cell voltage and current transients during 2h – rated discharge test cycles of cells with titanium-supported positive electrodes with 2 mm thick PAM. The data correspond to the cycle number interval #30 - #33.

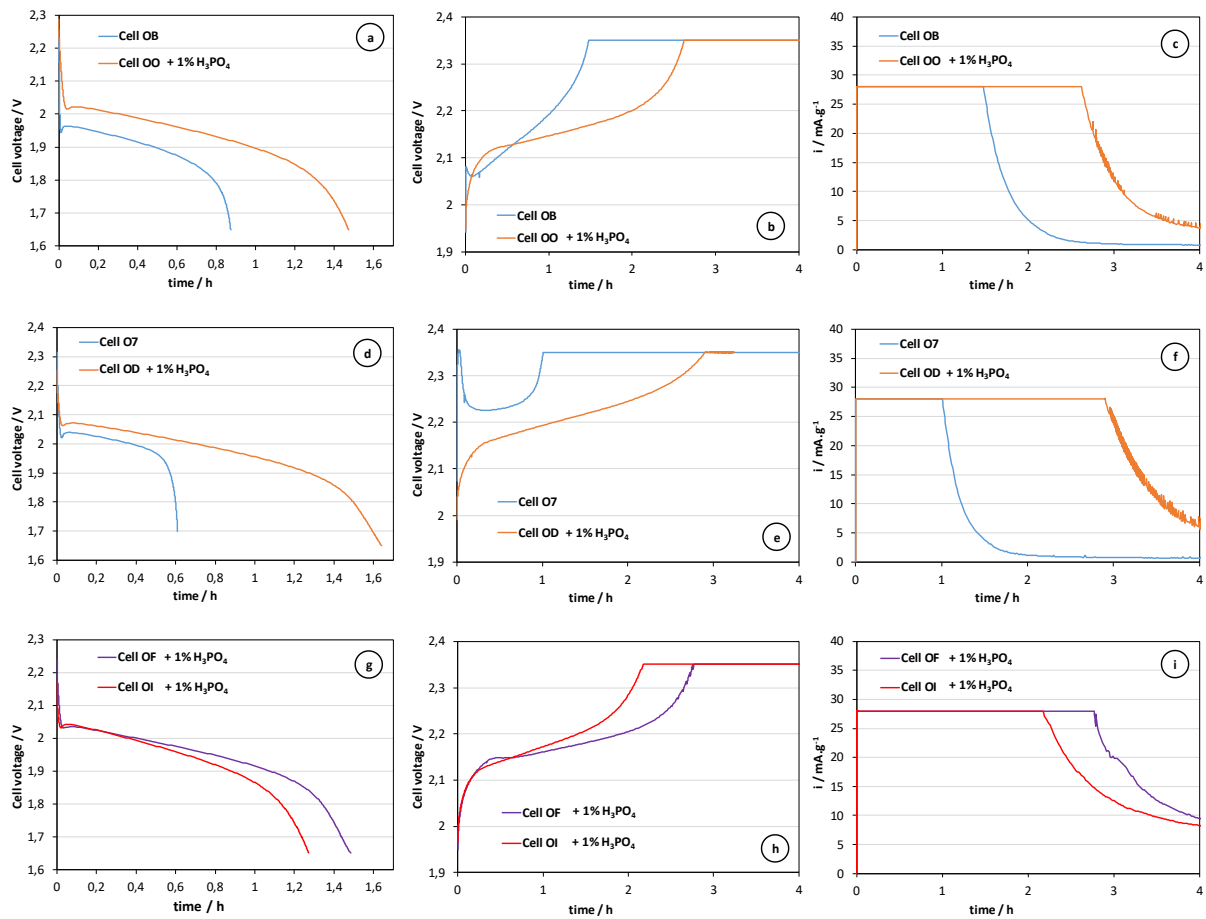


**Fig. 4.** Cell voltage and current transients during 2h – rated discharge test cycles of cells with titanium-supported positive electrodes with 1 mm thick PAM. The data correspond to the cycle number interval #30 - #33.

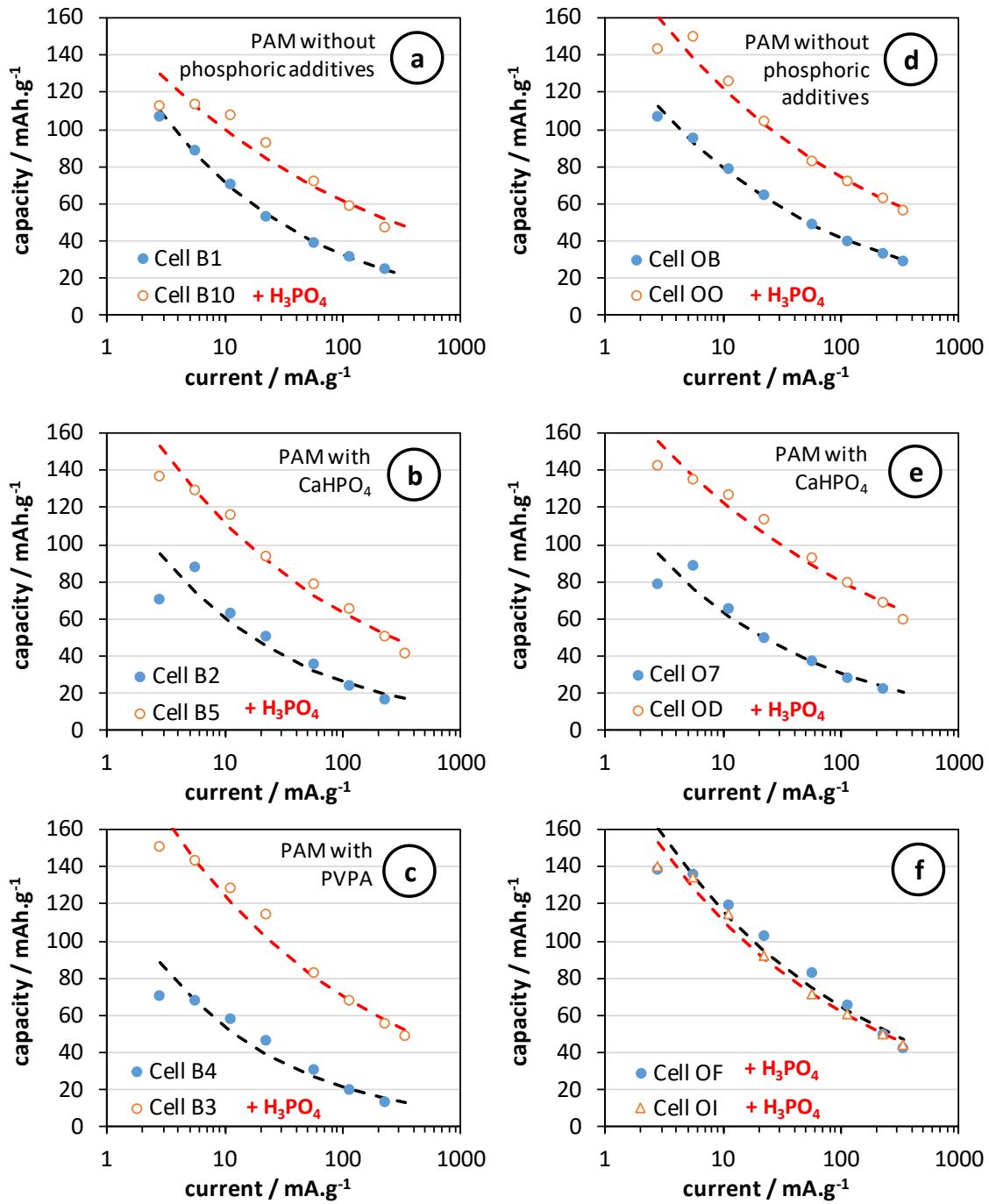


**Fig. 5.** Dependence of the discharge capacity on the discharge current and its correlation with the Peukert equation for cells containing pristine electrolyte and  $H_2SO_4$  doped with  $H_3PO_4$ .

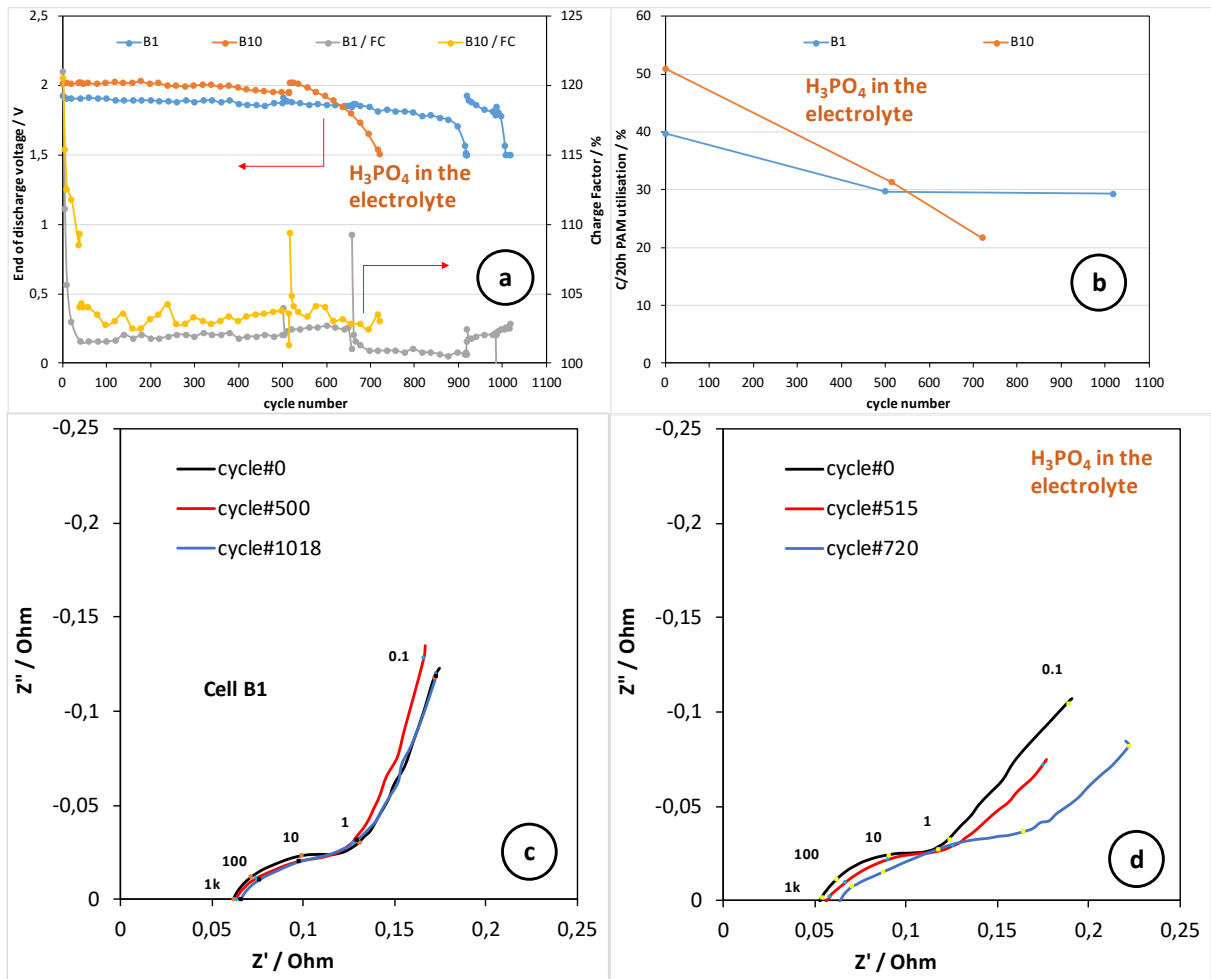


**Fig. 6.** Summary of the ageing testing of titanium-supported electrodes with 2 mm thick PAM without phosphate additives.

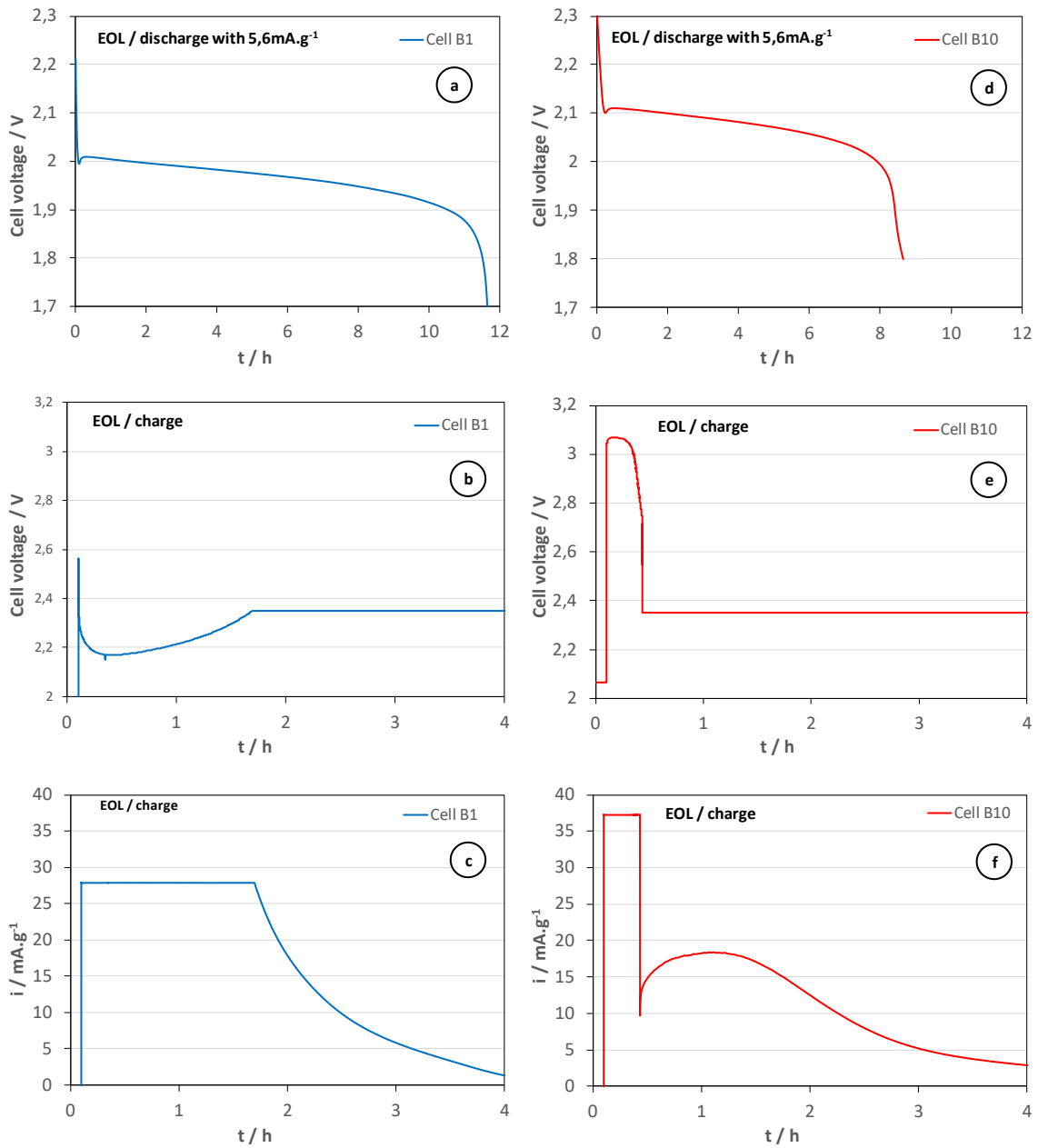


**Fig. 7.** End-of-life cell voltage and current transients during 20h – rated discharge test cycles of cells with titanium-supported positive electrodes with 2 mm thick PAM without phosphate additives.

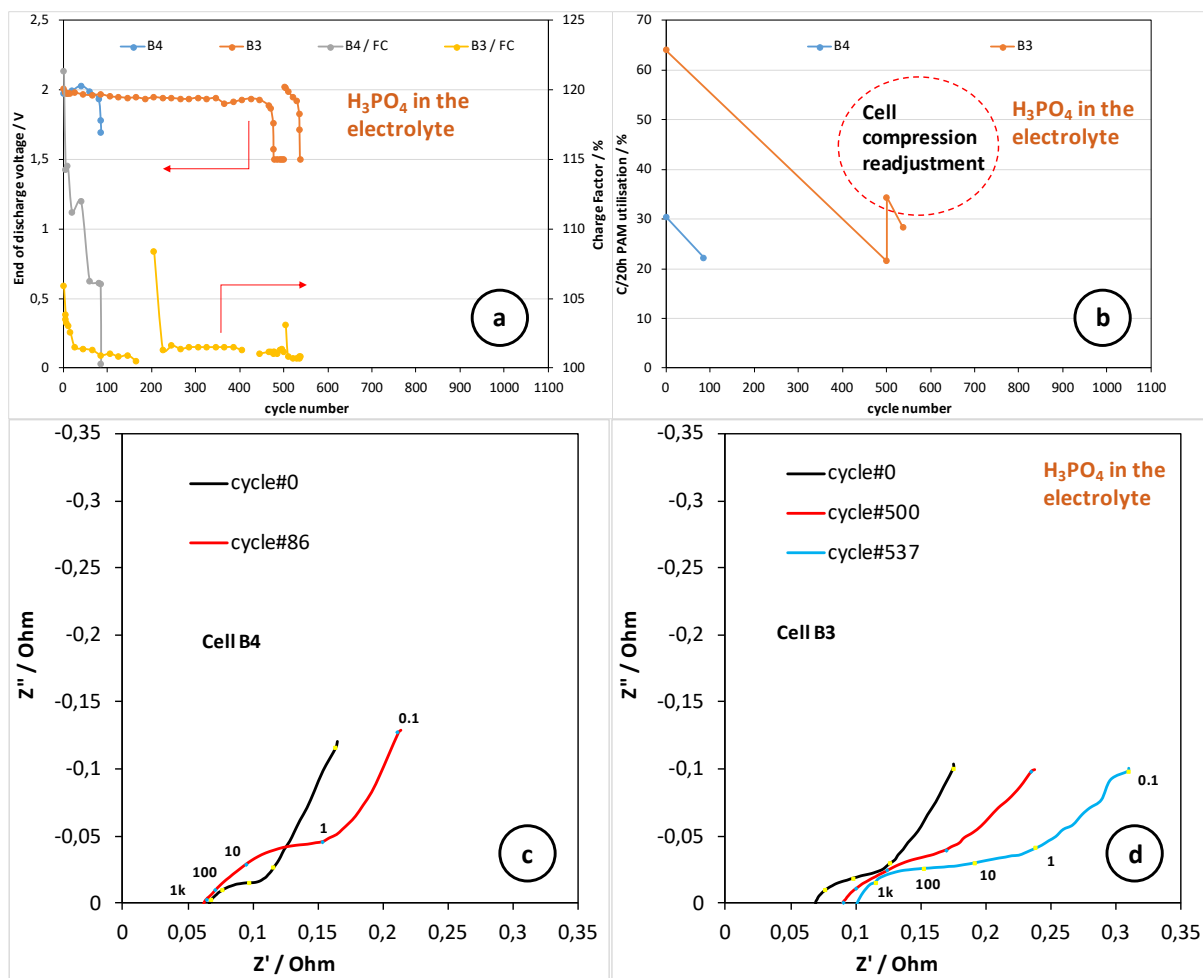


**Fig. 8.** Summary of the ageing testing of titanium-supported electrodes with 2 mm thick PAM containing PVPA additive.

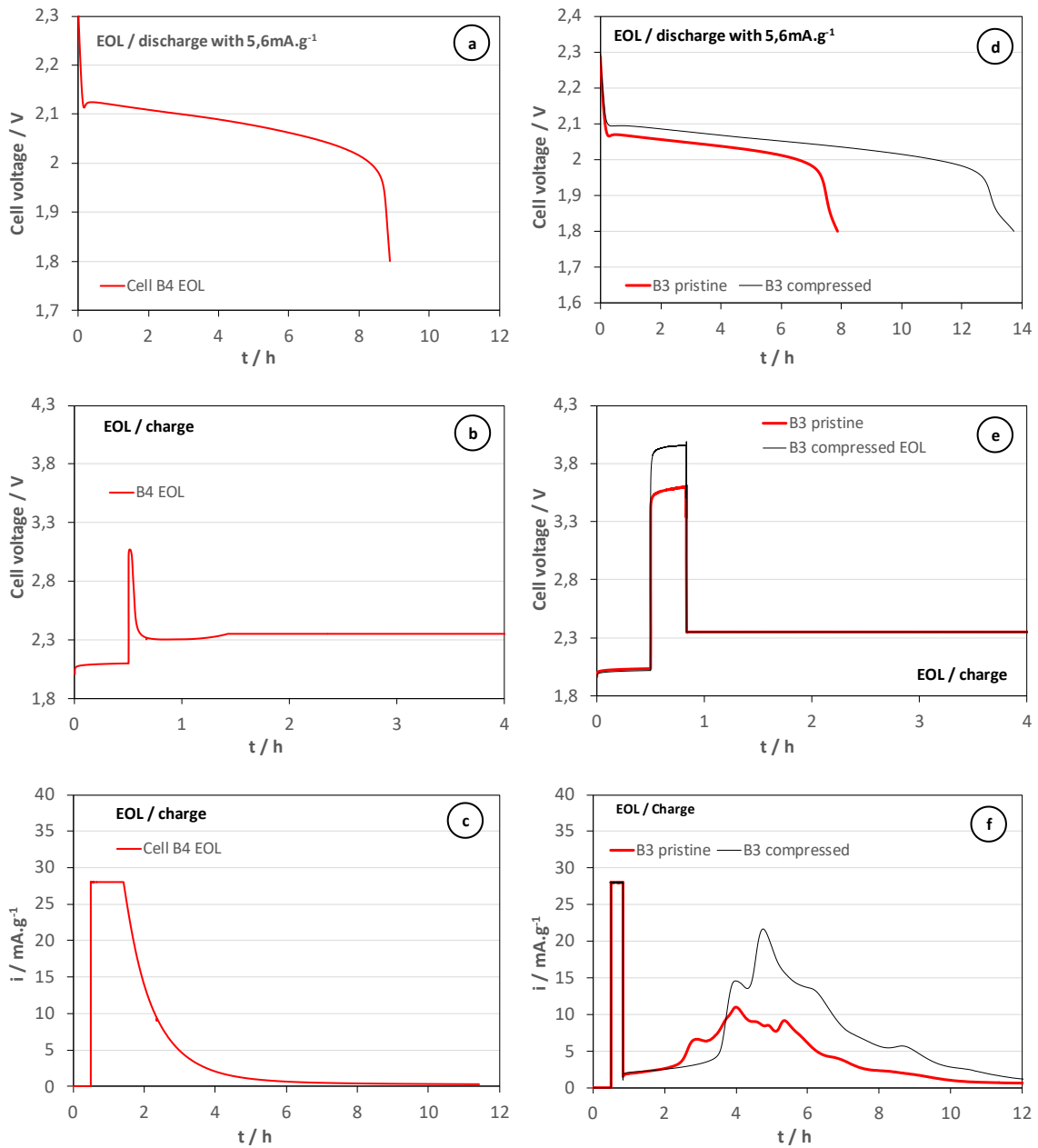


**Fig. 9.** End-of-life cell voltage and current transients during 20h – rated discharge test cycles of cells with titanium-supported positive electrodes with 2 mm thick PAM containing PVPA additive.

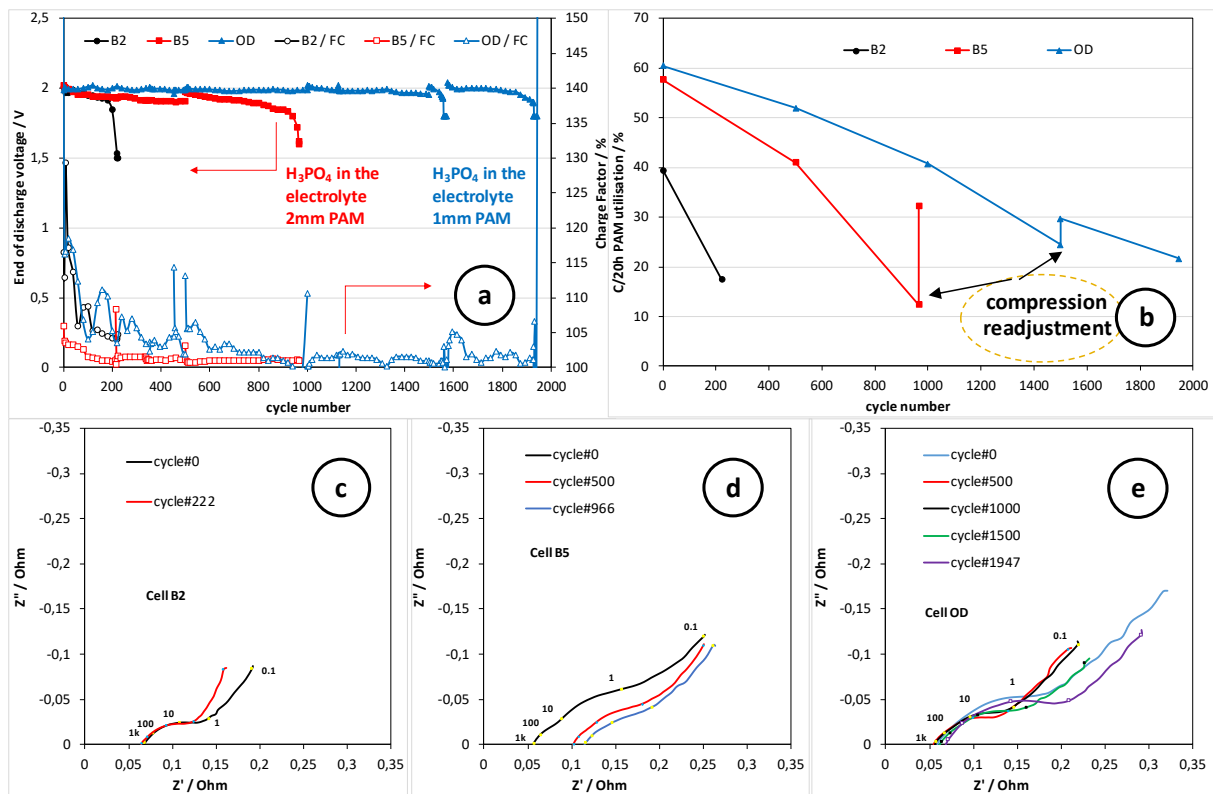


**Fig. 10.** Summary of the ageing testing of titanium-supported electrodes with PAM containing  $\text{CaHPO}_4$  additive.

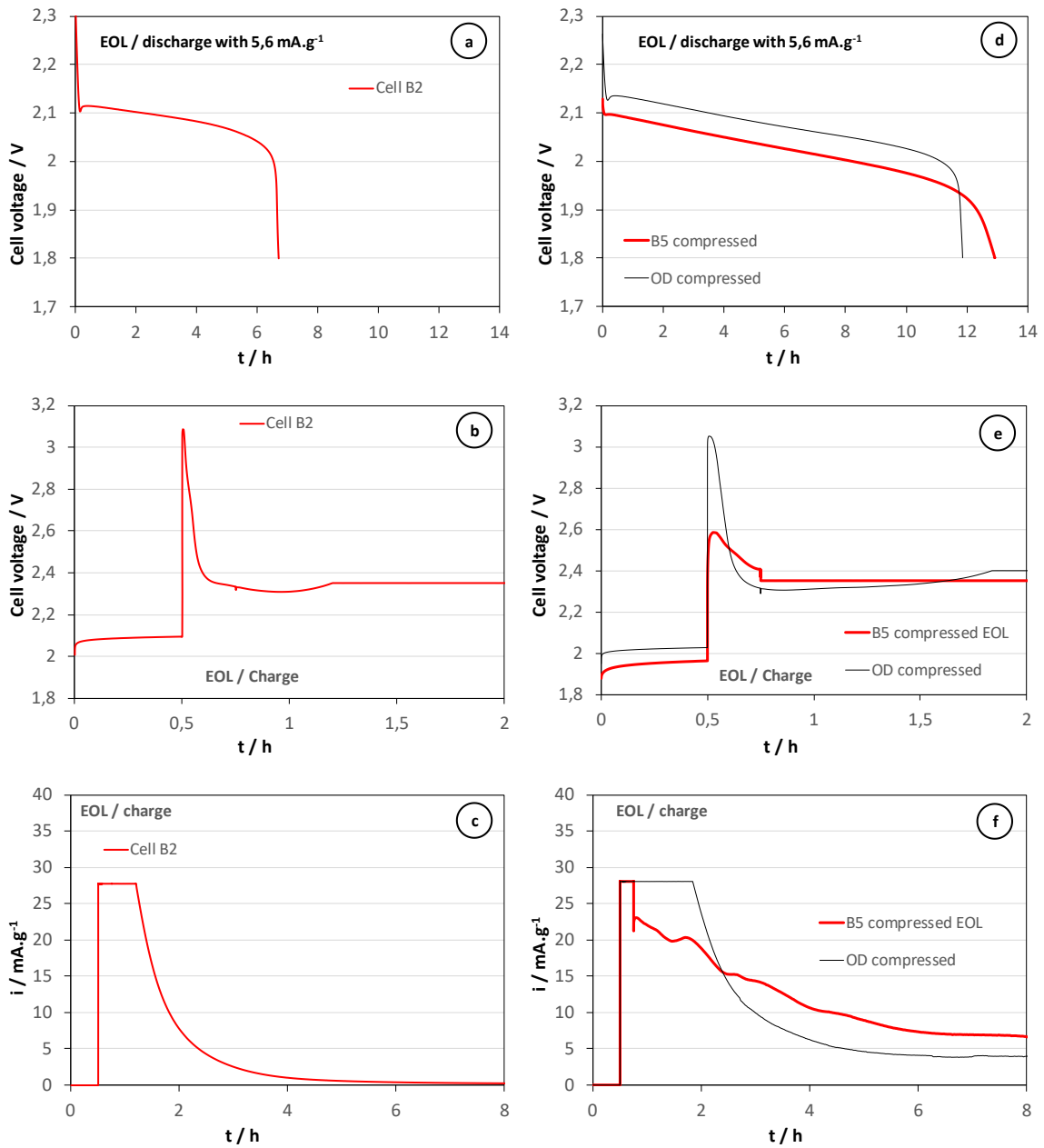


**Fig. 11.** End-of-life cell voltage and current transients during 20h – rated discharge test cycles of cells with titanium-supported positive electrodes with PAM containing CaHPO<sub>4</sub> additive.

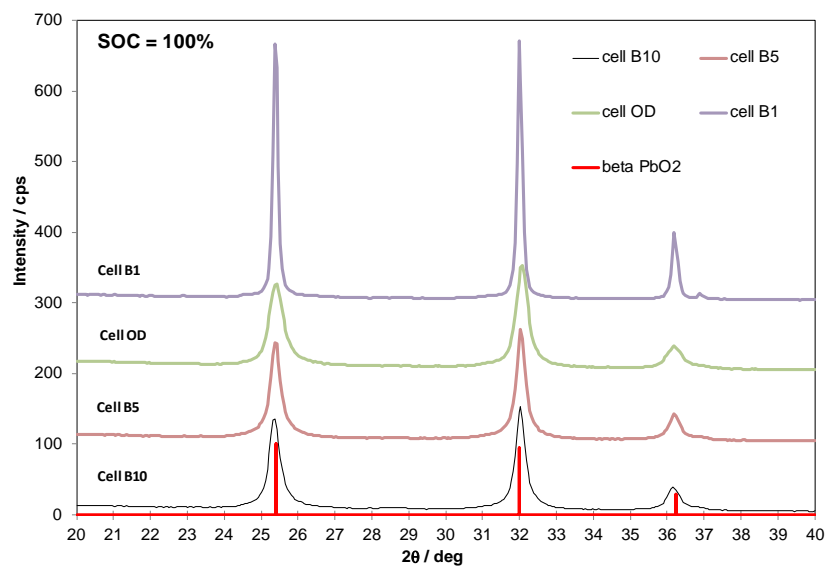


**Fig. 12.** X-ray diffraction patterns of PAM from aged cells formed and operated in electrolyte with and without an addition of H<sub>3</sub>PO<sub>4</sub>.

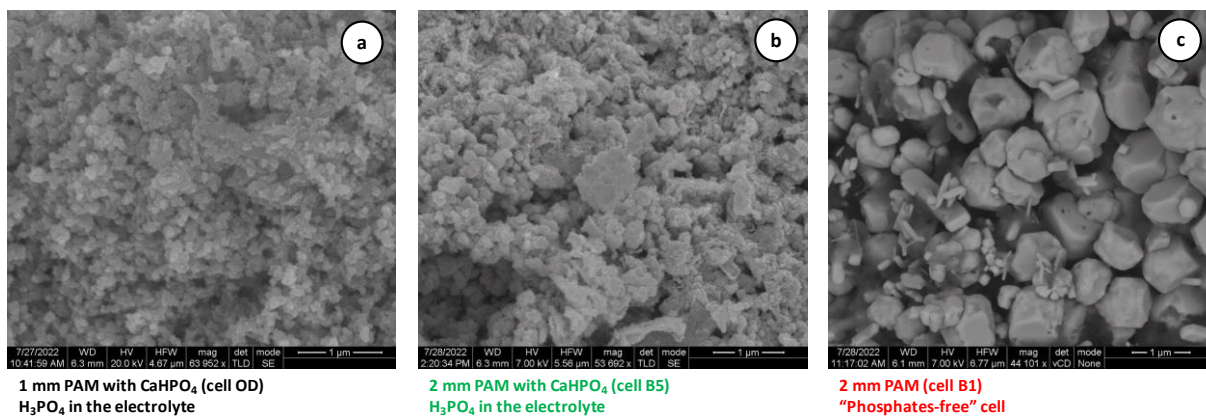


**Fig. 13.** Scanning electron micrographs of PAM from aged cells formed and operated in electrolyte with and without an addition of H<sub>3</sub>PO<sub>4</sub>.

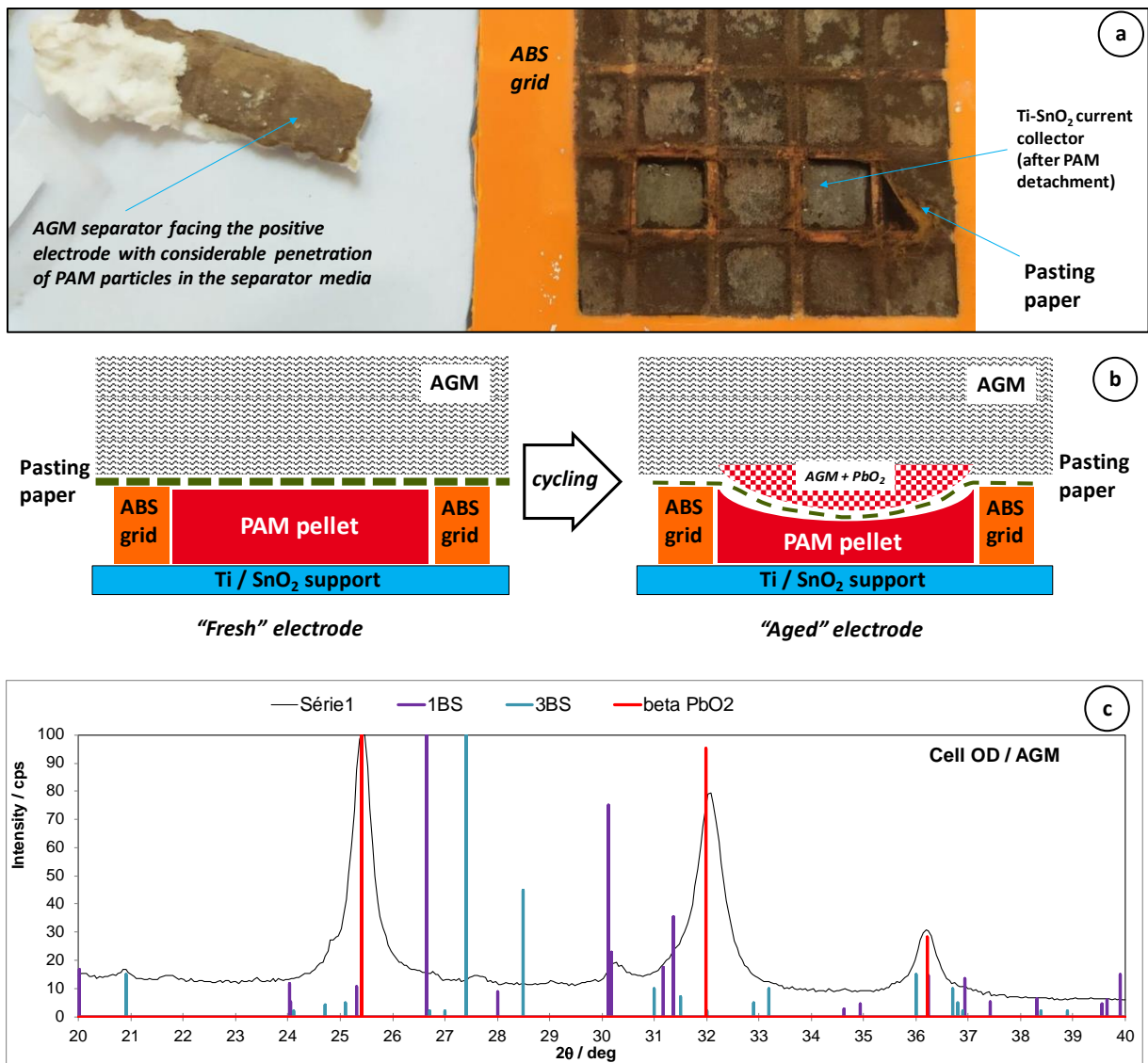


**Fig. 14.** Close-up image of electrode with 1mm thick PAM containing CaHPO<sub>4</sub> after the formation and cycling in electrolyte containing H<sub>3</sub>PO<sub>4</sub> and its interface with the AGM separator (a). Scheme of the evolution of the PAM pellet profile at the end of life of the cell (b). X-ray diffraction patterns of the brown material infusing the AGM separator at the PAM/AGM interface (c).

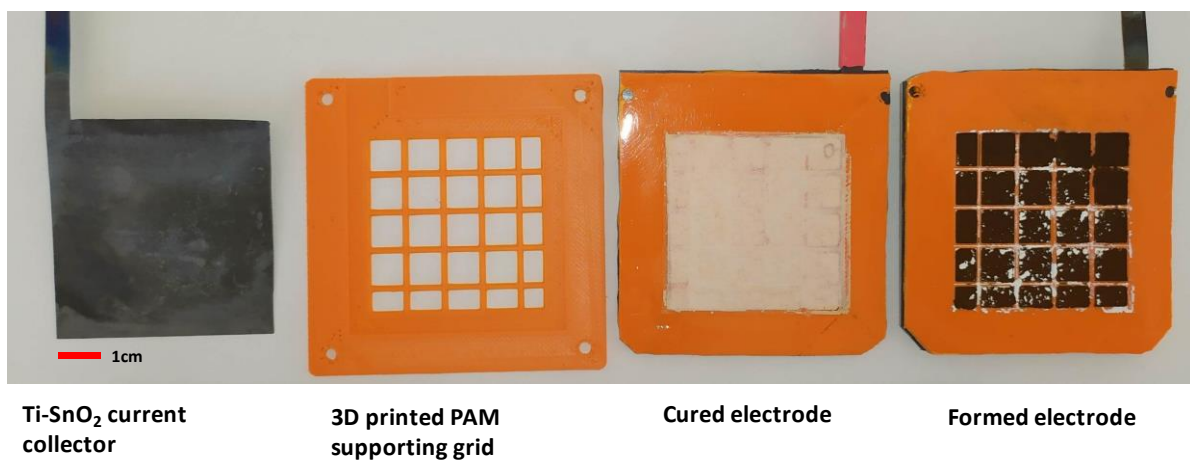
## Phosphoric acid activation of titanium-supported lead dioxide electrodes for bipolar battery applications

A. Kirchev\*, L. Serra, B. Marie

Univ. Grenoble Alpes, CEA, Liten, Campus Ines, 50 Av. de Lac Leman, 73375 Le Bourget du Lac, France

\*corresponding author e-mail: angel.kirchev@cea.fr

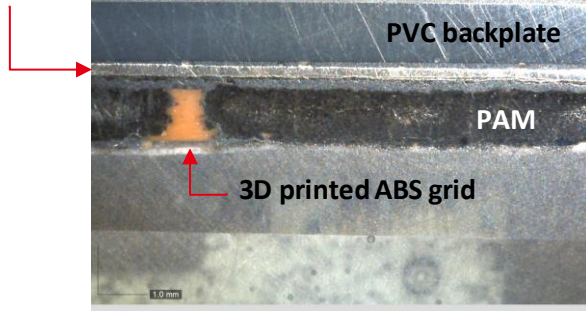
Supplementary information



**S1.** Image showing the principal components and stages of the titanium-supported electrodes studied in the present work.

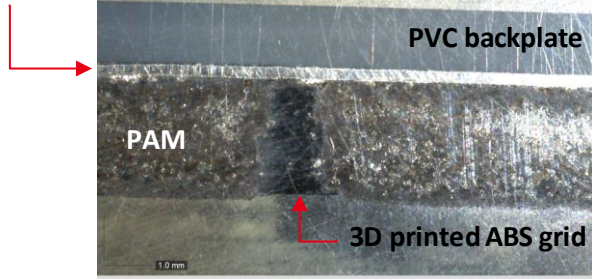
### Electrode with 1 mm thick PAM

Ti foil  
0,25mm

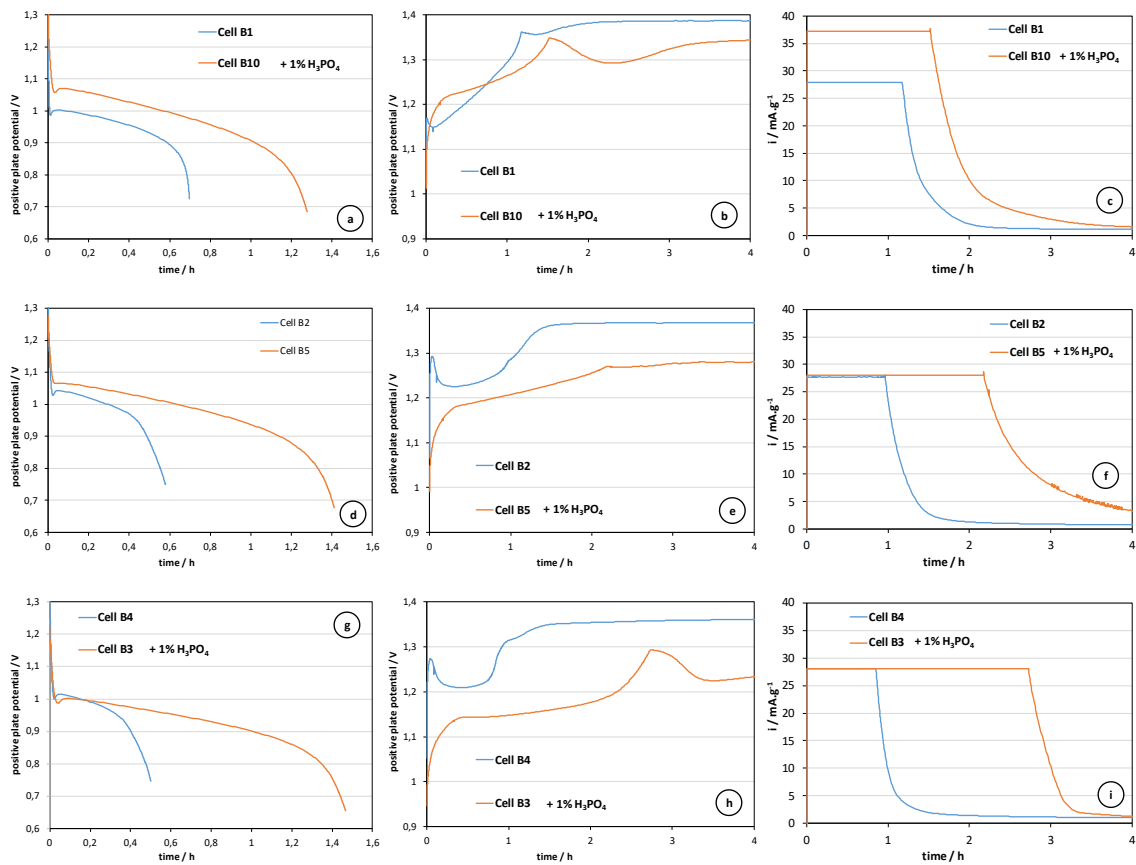


### Electrode with 2 mm thick PAM

Ti foil  
0,25mm



S2. Digital micrographs of the titanium-supported electrodes cross-section.



**S3.** Evolution of the positive plate potentials corresponding to the experiments presented in Figure 4.